Lagrangian eddy tracking reveals the Eratosthenes anticyclonic attractor in the eastern Levantine basin

Alexandre Barboni[1,2], Ayah Lazar[3], Alexandre Stegner[1], and Evangelos Moschos[1]

[1]Laboratoire de Météorologie Dynamique, Ecole Polytechnique, 91128 Palaiseau, France
[2]Département de Géosciences, Ecole Normale Supérieure de Paris, 24 rue Lhomond, 75005 Paris, France
[3]Israel Oceanographic and Limnological Research, Hubert Humphry St, Haifa, Israel

Correspondence: Alexandre Barboni (alexandre.barboni@polytechnique.edu)

Abstract. Statistics of anticyclonic eddy activity and eddy trajectories in the Levantine basin over the period 2000-2018 are analyzed using the DYNED-Atlas, which links the automated mesoscale eddy detection by the AMEDA algorithm with in situ oceanographic observations. This easternmost region of the Mediterranean sea, delimited by the Levantine coast and Cyprus, has a complex eddying activity, which has not yet been fully characterized. In this paper we use Lagrangian tracking
5   to investigate the eddy fluxes and interactions between different subregions in this area. The anticyclonic structure above the Eratosthenes seamount is identified as hosting an anticyclone attractor, constituted by a succession of long-lived anticyclones. It has a larger radius and is more persistent (staying up to four years in the same position with successive mergings) from other eddies in this region. Quantification of anticyclone flux shows that anticyclones that drift towards the Eratosthenes seamount are mainly formed along the Israeli coast, or in a neighbouring area West of the seamount. The southeastern Levantine
10   area is isolated, with no anticyclone transfers to or from the western part of the basin, defining the effective attraction basin for the Eratosthenes anticyclone attractor. Colocalized in situ profiles inside eddies provide quantitative information on their subsurface physical anomaly signature, whose intensity can vary greatly from dynamical surface signature intensity. Despite interannual variability, the so-called Eratosthenes anticyclone attractor stores a larger amount of heat and salt than neighbouring anticyclones, in a deeper subsurface anomaly that usually extends down to 500 m. This suggests that this attractor could
15   concentrate heat and salt from this sub-basin, which will impact the properties of intermediate water masses created there.

1   Introduction

The circulation in the eastern part of the Mediterranean sea has not been investigated as extensively as the western part, and some aspects of its circulation are still a subject for scientific debate. Different pathways for the mean flow were proposed with notable differences in the Libyan gulf and the Levantine basin (LB) (Robinson et al., 1991; Hamad et al., 2006). Since
20   the satellite Sea Surface Temperature (SST) images in the 90's there is an overall agreement on the mean counter-clockwise surface circulation in the eastern Mediterranean basin, the Atlantic waters (AW) coming through the Strait of Sicily, following the Libyo-Egyptian coast and then continuing along the Levantine and Turkish coasts (Hamad et al., 2006).

The Levantine basin, defined as the part of the eastern Mediterranean east of 23° E and south of 37° N (Hamad et al., 2006),

appears to have a rather complex and turbulent circulation, particularly in its southeastern part, bound by the topography of Cyprus and the Egyptian and Levantine coasts. Extensive in situ oceanographic surveys were performed in the previous decades (Robinson et al., 1991; Brenner, 1993; Hayes et al., 2011), notably with the work of the POEM group, already detecting in the 80's some recurrent large long-lived (lasting longer than a year) anticyclonic structures: Ierapetra south-east of Crete and Mersa-Matruh offshore Egypt above the Herodotus trench, at approximate location 33.2°N, 32.3°E (see notably scheme from Robinson et al. (1991)). South of Cyprus, different authors proposed a multi-pole structure named "Shikmona", of which they named the most active feature the "Cyprus eddy" (Brenner, 1993; Zodiatis et al., 2010). However, limited in time coverage, these studies remained with a static perspective. Zodiatis et al. (2010) probably presents the most advanced vision from this approach with a hint of interannual variability. In the more recent hydrographic regionalisation review of Ayata et al. (2018), the anticyclonic structure south of Cyprus is called "Eratosthenes anticyclone", the name used hereafter.

The development of satellite observation, initially with the use of SST, enabled to identify some of these long-lived anticyclonic structures as accumulation areas for mesoscale eddies detached from the coast, already detected in the 90's (Millot and Taupier-Letage, 2005; Hamad et al., 2006). Later altimetry products of Sea Surface Height (SSH) such as AVISO/CMEMS with grid resolution on the order of the deformation radius helped to investigate the unsteady dynamics of mesoscale structures in the region. Although not detected in instantaneous views, a constant and strong AW flux also exists in the center of the eastern basin in a turbulent Middle-Mediterranean jet (MMJ) (Amitai et al., 2010). However, studies such as Amitai et al. (2010) used Sea Level Anomalies fields (SLA) and an Eulerian approach of turbulence instead of focusing on eddy individual behavior. Eddy climatology in the LB then remains unknown, and impact on water masses transport performed by such transient eddies has not been studied yet. Figure 1 presents the topography of the LB, overlaid with Mean Dynamic Topography (MDT) from 2000 to 2018 retrieved from CMEMS at a 1/8°resolution. The Eratosthenes seamount, whose summit is about 700m deep at approximately 33.7 ° N, 32.7 ° E, appears to be a prominent topographic feature in the basin and indeed displays a mean anticyclonic circulation with a closed contour of higher MDT, coherent with recent campaigns sampling the Eratosthenes anticyclone (Hayes et al., 2011; Moutin and Prieur, 2012). But some differences from previous studies also appear, as this eddy is shifted westwards from its former reported location closer to the Levantine coast, at approximately 33.5 ° N, 33.5 ° E (Brenner, 1993; Amitai et al., 2010) (under the name "Cyprus eddy"). Although there have been improvements in the SSH products since Amitai et al. (2010) (Taburet et al., 2019), this westward trend seems to be a physical displacement of the Eratosthenes anticyclone (Zodiatis et al., 2010).

Intense eddy activity in a basin with strong topographic constraints may lead to numerous eddy-eddy interactions, and highlights the need to take into account merging and splitting events between mesoscale structures. First eddy automated detection and tracking algorithms were mostly based on SSH fields and did not detect such interactions (Chelton et al., 2011; Mason et al., 2014). Over the past decades, numerous algorithms were further developed to take into account mergings and splittings, based on SSH (Matsuoka et al., 2016; Cui et al., 2019; Laxenaire et al., 2018) or a mixed velocity field-SSH approach (Yi et al.,

2014; Le Vu et al., 2018).

60

The AMEDA algorithm developed by Le Vu et al. (2018) is used in this study. It detects eddy centers by computing the Local Normalized Angular Momentum (LNAM) introduced by Mkhinini et al. (2014) - as opposed to Yi et al. (2014) using the Okubo-Weiss parameter - and computes the maximal tangential speed within the largest surrounding closed SSH contours to find eddy contours. Eddy observations at different timesteps are gathered in tracks by minimizing a cost function taking
65 into account spatial proximity but also changes in eddy size and intensity. Detection of merging and splitting events are next detected as the outcome of eddy interactions, when two eddies share a closed SSH contour with averaged velocity higher than for each eddy taken separately. The AMEDA algorithm was used successfully in various case studies, notably in the Algerian basin by Garreau et al. (2018) and in the Arabian sea by de Marez et al. (2019). Detection of mergings and splittings enables to reconstruct the eddy network, mesoscale structures not being independent but often interacting with each other. Following
70 this idea Laxenaire et al. (2018) was able to show the connection between Indian and Atlantic oceans through Agulhas rings crossing the Southern Atlantic. However if several studies did develop algorithms to detect eddy interactions, we are not aware of studies that have quantified nor analyzed the additional information from merging and splitting events in terms of eddy behavior, apart from Laxenaire et al. (2018).

75 Nevertheless, satellite analysis alone cannot reveal the subsurface structure. Moutin and Prieur (2012) for instance, studied three anticyclones in the Mediterranean sea with similar SLA signatures but discovered extremely different heat and salt integrated anomalies. In the LB, Gertman et al. (2010) discovered smaller scale eddies detaching from the Israeli coast through SST and drifters data, and Hayes et al. (2011) discovered a huge salt anomaly in the Eratosthenes anticyclone despite a weak SSH signature. These studies show the importance of in situ observations in addition to satellite data, but they were campaign-
80 specific instantaneous observations. Before eddy automated detection, Menna et al. (2012) conducted a statistical study of mesoscale interactions in the LB by adding in situ drifter velocities to SSH-derived velocities, but sampling was sparse and without vertical information. The large-scale deployment of autonomous drifters in the global ocean (such as the Argo or MEOP programs), as well as the centralisation of collected data (such as CMEMS products), enables to bridge the gap in the temporal scale between satellite and in situ data. Argo is a global array of more than 3000 floats measuring temperature and
85 salinity down to 2000 m (ARGO, 2020). Using Argo data, Laxenaire et al. (2019) captures the subsurface evolution of one single Agulhas ring over 1.5 years in the South Atlantic ocean with the conjunction of Argo profiles and SSH data. It demonstrates that long-lived anticyclones can transport warm water masses over very long distances isolated in their thick core. Recently in the Algerian basin (Pessini et al., 2018) attempted to link eddies observations with in situ measurements and to compute eddy regional statistics, but with an algorithm not taking into account merging and splitting events. (Mason et al., 2019) also
90 attempted a study of the vertical eddy structure with regional variation in the Alboràn sea, but on data from assimilated models. Such regional characterisation of eddy systematic detection has not been attempted so far in the Eastern Mediterranean.

This approach of both eddy tracking, detected by altimetry taking into account mergings and splittings, and colocalisation with in situ observations can be generalized into an eddy atlas. The DYNED-Atlas combines over 19 year of subsurface observations from Argo floats to identified eddies, tracked in time and space by the AMEDA algorithm (DYNED-Atlas-Med, 2019). The DYNED-Atlas is the perfect tool for the study of eddy dynamics and associated transport of water masses in their cores, as it combines eddy detection and physical properties. It has not been exploited in the LB yet, although Stegner et al. (2019) already demonstrated very deep subsurface eddy signatures in this area.

Using eddy contours, tracks and colocalized profiles from the DYNED-Atlas, extended with available XBT and CTD profiles to compensate sparsity of observations, this study will investigate additional information from Lagrangian anticyclone tracking and statistically significant drift pattern and structures in the Southeastern LB - East of 28°E and South of Cyprus. After introducing the datasets in Sect. 2, we present our methodology of a Lagrangian convergence framework and the regions studied in Sect. 3. Analysis of this method with the DYNED-Atlas data are detailed in Sect. 4. Next vertical structure oceanographic observations colocalized inside eddies are used to study the eddy vertical signatures (Sect. 5). Possible mechanisms at work and hydrographic effects are discussed in the last part.

2 Data

2.1 Eddy contours, centers and tracks

The dynamical evolution of eddies and their individual tracks are retrieved from the DYNED-Atlas data-base (DYNED-Atlas-Med, 2019) for the period 2000 to 2018. The DYNED-Atlas project with eddy tracks and physical properties signature is accessible online: https://www1.lmd.polytechnique.fr/dyned/. The dynamical characteristics of the eddies contained in the DYNED-Atlas database were computed by the AMEDA eddy detection algorithm (Le Vu et al., 2018) applied on daily surface velocity fields. The latter were derived from the Absolute Dynamic Topography (ADT) maps produced by Salto/Duacs and distributed by the Copernicus Marine Environment Monitoring Service (CMEMS) with a spatial resolution of 1/8°, on the order of the internal deformation radius in the Mediterranean sea (10 to 12 km, Mkhinini et al. (2014)). A cyclostrophic correction is applied on these geostrophic velocities to accurately quantify eddy dynamical properties (Ioannou et al., 2019). Unlike standard eddy detection and tracking algorithms, the main advantage of the AMEDA algorithm is that it detects the merging and the splitting events (Le Vu et al., 2018), which allows to build a network of trajectories associated to each eddy. In other words, we can thus reconstruct its "genealogy".

2.2 Remote sensing measurements

To compute the MDT over the 2000-2018 period we use the daily high-resolution (1/8°) AVISO ADT delayed-time product provided by the CMEMS, under product name SEALEVEL_MED_PHY_L4_REP_OBSERVATIONS_008_051. This altimetry gridded product is also used to locate the in situ CTD or glider measurements in comparison with the characteristic eddy

contours in section 5. Otherwise, to confirm more precisely the location of eddies and their size some specific days, we use
the high-resolution (1/120°) merged-multisensor SST data representative of nighttime values, provided by the CMEMS under
product name SST_MED_SST_L3S_NRT_OBSERVATIONS_010_012.

2.3 In situ oceanographic observations

About 34406 Argo profiles are available from the DYNED-Atlas in the whole Mediterranean sea over this 19-year period.
Nevertheless, due to sparser campaigns only 9384 were available in the LB, and mostly after 2014. To complete these in situ
measurements, we add 2311 CTD and 3860 XBT casts downloaded from the SeaDataNed portal (https://www.seadatanet.org/
Data-Access, data in unrestricted access), and 7020 additional profiles from the CORA database, also available on the CMEMS
catalogue with reference INSITU_GLO_TS_REP_OBSERVATIONS_013_001_b. Finally, a glider of the Israel Oceanographic
and Limnological Research (IOLR) through one transect performed offshore Israel in October 2018 measured 370 profiles that
were added to the database. The above add up to 22945 profiles from 2000 to 2018 in the LB. All the hydrological profiles
are then colocalized with detected eddies following the standard procedure used in the DYNED-Atlas data-base. Profiles are
considered to be inside an eddy if they are inside its maximal speed contour.

3 Methodology

As opposed to previous studies that either considered eddy activity from "building-block" structures (Robinson et al., 1991)
or Eddy Kinetic Energy (EKE) fields derived from SLA compared to a MDT (Amitai et al., 2010), we follow here eddies
as daily, individual detections gathered in tracks. Eddies are not only active as individuals but also as a network of turbulent
structures interacting with each other. Hence the importance of taking into account merging and splitting events to reconstruct
this network. This approach then aims to quantify eddy transfers between different subregions. It is similar and greatly inspired
by the previous work done by Laxenaire et al. (2018) for Agulhas rings in the South Atlantic ocean.

3.1 Lagrangian convergence framework

We define here a framework to count eddy transfers imported to and exported from a studied region, whose successive steps
are shown in Fig. 2. The Eratosthenes seamount region, studied as an example in the above figure, is bordered with a green line
(coordinates in Table A1).

On one hand we consider *importing* eddies the eddies being part of the family tree coming into a region. The *order zero*
eddies are defined as the ones converging directly to the region (trajectories as blue lines in Fig. 2a). This *order 0* label en-
compasses mainly eddies dying within the studied region; however, some eddies can stay stationary for a very long period in
the same area, later moving and dying in another place. In order to take them into account, the definition of an eddy labelled
as *order 0* is an eddy dying or spending more than half of their lifetime inside the perimeter of the studied region. Sensitivity
of this 50% lifetime criterion is detailed in Fig. A1 in appendix, and this definition does not lead to inaccurately count as

155   *importing* eddies the ones which are just transiting. Indeed eddies labelled as *order 0*, when getting out of the studied region, disappear in the immediate vicinity (see an example in Fig. A2 in appendix) . Next, we label as *order 1* the eddies that merge with an *order 0* eddy (Fig. 2b, cyan lines). Recursively, we label as *order 2* the eddies that merge with an *order 1* eddy (not shown in Fig. 2, but in Fig. 6a). Hereafter we will discard from the discussion *orders* higher than 2, as their quantity was found to be negligible.

160

    On the other hand an *exporting* eddy flux moves some eddies outside of the region. We distinguish two categories of *exporting* eddies: (1) if two eddies undergo a splitting event and one of the split eddies spends more than half of its lifetime outside the region, it is considered an *exporting split* eddy; (2) if an *order 0* eddy dies while merging with external eddies which themselves drift away from the region, this external eddy is considered an *exporting merging* eddy. Exporting split (yellow dashed lines) and merging (red dashed lines) eddies are shown in the example in Fig. 2c; however none of the latter case were detected for this particular region.

    It should be noted that in this framework, the *order 0* label prevails on other labels defined: if an eddy meets criteria for both *order 0* and *order 1*, it is labelled as *order 0* only. Additionally *exporting (split and merging)* eddies are labelled as such only if they are not already labelled as an *importing* eddy. It should also be noted that eddies labelled as *order 0* can be born within or outside the given region. Lastly, a label is relative to a region: an eddy spending more than half of its lifetime in a region but drifting and dying in another is labelled as *importing order 0* for both regions (see discussion about Table A2 in Sect. 4.2). In this framework and in the figures hereafter, *importing* eddies are plotted at their appearance location as black dots with size proportional to the eddy lifetime to show the origin of the water masses. *Exporting split* and *merging* eddies are plotted at their disappearance location as squares, also lifetime-scaled. Trajectories are smoothed through a (10 km x 10 km) window. Color chart is summarized in Fig. 2d and used throughout this study.

    At last, attractiveness of a region for eddy - for a given polarity - is estimated in the *net eddy gain*. This is the total number of *importing* eddies - the sum of *orders 0-1-2* and possibly higher - minus the number of eddies already born in the region of interest. This gain is later shown in Table A2 and discussed in Sect. 4.2.

3.2   Definition of anticyclonic and cyclonic regions

To study further the exchanges between eddying structures in southeastern part of the LB, eight regions of interest are considered and shown in the MDT of Fig. 3. These regions are defined as close as possible to non-overlapping rectangular shapes, tiling as much as possible of southeastern corner of the LB ($\approx 78\%$ of the attraction basin discussed in Sect. 4.3 is covered) and with similar size (areas and coordinates provided in Table A1 in appendix). Each box is defined to correspond to a structure showing up in the MDT. An average cyclonic (respectively anticyclonic) activity can be inferred, if it encompasses a depression (a hill) in the MDT, and hereafter we refer to these regions as cyclonic (CY) (respectively anticyclonic (AC)) regions: "Beyrut" (AC), "Haifa" (CY), "Tel-Aviv" (AC), "Port-Saïd" (CY), "Herodotus" (AC), "Nile" (AC) and "Eratosthenes" (AC,

already shown in Fig. 2). Although not in our focus region, a comparison is also done in Sect. 4.5 about the "Mersa-Matruh" (AC) region. The eight distinct regions are presented on Fig. 3 with red (green) borders in solid lines for CY (AC) regions. The attraction basin of the Eratosthenes region (see Sect. 4.3) is shown with a dashed line.

3.3 Eddy-induced physical property anomalies

The DYNED-Atlas establishes a method to estimate the physical property anomalies induced by an eddy (DYNED-Atlas-Med, 2019). This method is followed in this study, only extending the database with profiles form other sources than Argo, and using *in situ* temperature instead of potential temperature to match up with XBT profiles. Each oceanographic measurement is compared to the AMEDA observations. If it falls within the contour of an eddy on the same day it is cast, the profile is colocalized with the eddy and then considered as sampling its physical properties. If it falls outside any eddy observation, it is then considered *outside-eddy*. Estimation of the eddy-induced physical property anomalies (temperature, salinity, density) is next done by comparison with a reference background. For each observation, a climatological background is then computed by averaging all *outside-eddy* profiles from 2000 to 2018, at a distance smaller than 150 km from the its cast position and at the same season (within a ±30 days period whatever the year). It is intended to be more statistically significant than estimates performed during a single campaign, usually through one profile inside an eddy and another one outside (e.g. Moutin and Prieur, 2012).

4 Lagrangian tracking results

4.1 Eddy activity from a Lagrangian framework

Figure 4 presents eddy occurrence and drift in the LB for anticyclones and cyclones, with the designated regions of Fig. 3. Time occurrence percentage, shown in colors, is computed as the time spent inside the maximal speed contour of a detected eddy, whereas the drift, shown with arrows, is the mean speed of eddy centers passing through the pixel. Pixel size is (1/8°x 1/8°). A Gaussian smoothing is performed (kernel size 5x5 pixels), and data from pixels crossed by less than 5 eddy centers are discarded. This picture can be seen as an eddy Lagrangian approach equivalent to the MDT shown in Fig. 1 and 3, adding new information. Firstly, the spatial distribution of cyclonic and anticyclonic eddies is extremely non-homogeneous: almost no anticyclones are present in the northern part of the LB. The prevalence of the Mersa-Matruh and Eratosthenes structures as persistent anticyclones is confirmed with coherent spots hosting anticyclones more than 50% of the 2000-2018 time period. Cyclones are present in the southeastern part of the LB, in particular in the "Haifa" region. All *anticyclonic* (respectively *cyclonic*) regions do have on average a higher presence of anticyclones (cyclones), confirming through a Lagrangian approach the regions defined in Sect. 3.2. Comparison in Fig. 4 with the Ierapetra eddies Southeast of Crete highlights the difference between Lagrangian and Eulerian visions. The Ierapetra eddies show up very clearly in SLA maps and are the most intense eddies in the region (Amitai et al., 2010). However as they do not have fixed stable position and can drift far away after their formation (Ioannou et al., 2017), they form a less concentrated spot in Fig. 4. The Lagrangian vision then shows more persistent

220 yet maybe less intense structures.

Additionally Fig. 5 shows eddy lifetime statistics in the LB, with a comparison of the normalized cumulative eddy lifetime, i.e. the probability for an eddy to live longer than a given time period. In the Mediterranean sea, the lifetime for cyclones is on average far shorter than for anticyclones, as already shown by Mkhinini et al. (2014). However this disequilibrium is even 225 more pronounced in the LB: the cyclones lifetime distribution is very similar than in the rest of the Mediterranean, whereas anticyclones clearly tend to live longer. As an example, in absolute units of detected eddies, 105 anticyclones (out of 5770) compared to 70 cyclones (out of 7159) are found to live longer than 400 days in the whole Mediterranean, whereas in the LB 39 anticyclones (out of 1210) compared to 17 cyclones (out of 1630) live longer than 400 days. The intense Ierapetra anticyclones have been shown to live often more than 3 years (Ioannou et al., 2017), but as no more than one of these eddies is formed each 230 year they can not explain alone this trend of longer anticyclone lifetimes. These statistics suggest the existence of mechanisms prolonging anticyclones lifetime in the LB. Hence, this study focuses particularly on anticyclones, whose longer lifetimes also lead to capture water masses in their core for an extended period and have higher hydrologic impact.

4.2 Inter-region anticyclone transfers

The Lagrangian convergence framework detailed in Sect. 3.1 is applied in Fig. 6 to the 7 regions of the Southeastern LB 235 (Eratosthenes, Beyrut, Haifa, Tel-Aviv, Port-Saïd, Herodotus and Nile, Mersa-Matruh being studied later in Sect. 4.5), only considering anticyclones (statistics also shown in Table A2). The color code is the same as in Fig. 2 and reminded in panel 6h. For each panels of Fig. 6 all other regions are shown, with green (respectively red) borders for AC (CY) regions. The region to which each panel title refers is outlined with a thicker line. For all AC regions (Fig. 6a-b, 6d, 6f-g), anticyclones trajectories form a rather concentrated bulk at the center of the region, whereas CY regions (Fig. 6c and 6e) have only a very sparse and 240 random anticyclone occurrence. The mean dynamical activity from Sect. 3.2 is confirmed, as only AC regions host a preference spot for anticyclones, whereas CY regions tend to be avoided by anticyclones.

Important differences can however be noted between AC regions. In the Beyrut region, anticyclones meander a lot but have few interactions (only 2 mergings and 2 splittings in 19 years) and eddies have a moderate lifetime there (126 days). In the 245 Tel-Aviv region, anticyclones are more short-lived (97 days on average), spend less time in the region with few meanders and 4 merging exports were recorded for the benefit of the Eratosthenes region; this characterizes the Tel-Aviv region rather as an anticyclone formation region. Characterizing the Herodotus region is more difficult, as some eddies stem from the Nile region and some others eventually merge with Eratosthenes region long-lived anticyclones; this regions seems to act as an anticyclone formation region (42 anticyclones born there) but also transitory to the Eratosthenes one, with which it interacts a lot with 250 8 merging exports. On the contrary, the Nile region is a strong and preferred anticyclonic spot but eddies there interact very little with neighbouring regions; the Nile region acts rather as a termination region for anticyclones formed to the West and following the Libyo-Egyptian coast.

Nonetheless, some anticyclones are formed inside CY regions, notably in the "Haifa" region. In this region anticyclones are often short-lived (average lifetime 94 days) and often disappear while being exported to the Eratosthenes region (6 mergings recorded); the role of the Haifa region is then similar to the Tel-Aviv region acting as a region of anticyclone formation. The case of the Port-Saïd region is more ambiguous, no clear pattern being visible. Statistics in appendix (Table A2) seems to show it attracts some anticyclones, but this can be due to the fact that some long-lived eddies of the Eratosthenes region do sometimes venture approximately hundred kilometers farther south. This ambiguity also shows limits of this Lagrangian approach, as it is sensitive to singular event for eddies living sometimes longer than 3 years. As a comparison, Fig. A3 in the appendix shows the same analysis as Fig. 6b for the Haifa region but studying cyclone transfers. Patterns for cyclones are less clear than for anticyclones, likely because cyclones live shorter and are thus more numerous. However it confirmed the Haifa region as a stable spot for cyclones.

4.3 Eratosthenes anticyclone attractor (EAA)

Fig. 7 and Table A2 summarize anticyclone transfers in the Southeastern LB. Attractiveness of each region is measured through the *net eddy gain* introduced in Sect. 3.1. Arrows in Fig. 7 indicate eddy transfers, with thickness proportional to the number of eddies transferred. The particular case of the Eratosthenes region shows a clear convergence with 44 *importing* anticyclones attracted whereas only 14 were initially born in this region surrounding the Eratosthenes seamount, from 2000 to 2018, hence a *net eddy gain* of +30 and an approximate anticyclone flux of more than one merging per year. Instead of freely drifting westwards as expected by the β-drift (Chelton et al., 2011), anticyclones tracks shown in Fig. 2b (or alternatively Fig. 6a) reveal that eddies meander a lot over the high bathymetry, as shown by the density of blue tracks, seemingly trapped by the seamount. On the over hand only few *exporting split* eddies escape and not a single *exporting merging* eddy is detected; these split eddies are even more short-lived, as shown by the small size of the disappearance square (Fig. 2c). This trend of a high *net eddy gain* together with few *exporting* eddies and the persistent anticyclonic activity int the Eratosthenes region (Fig. 4) allows to identify this region as hosting an anticyclone attractor, called hereafter the *Eratosthenes anticyclone attractor* (EAA).

Moreover this observed convergence toward the Eratosthenes seamount seems to be geographically bounded, tracks in Fig. 2a-b showing that anticyclones come from as far as 300 kilometers away, but with a distinct westward limit, depicted with a black dashed line. This area of anticyclones converging to the EAA, although constrained by topography, swaps a large part of the southeastern LB and is called the EAA *attraction basin* in this study, and reminded in Fig. 3, 4, 6 and 7. It is defined as a straight line ranging from the Egyptian city of Alexandria (31.0° N, 29.6 ° E) to the Cypriot city of Paphos (34.8 ° N, 30.4 ° E) with a break angle at 33.2 ° N, 30.4 ° E, and a second line closing it between the Greek Cape on Cyprus island (35.0 ° N, 34.1 ° E) to the Lebanese city of Tripoli (34.4 ° N, 35.8 ° E).

Finally Fig. 8 analyses the anticyclones constituting the EAA (i.e. *order 0 importing* anticyclones for the Eratosthenes region, shown in blue lines in Fig. 6a). The upper panel presents their timeseries, with the color indicating when the center is inside or outside the region. An anticyclone is always present inside, with relay between long-lived eddies: each time an

anticyclone inside the region dies, it is replaced by another, leading to only about 1 year out of 19 without an anticyclone over the Eratosthenes seamount. Anticyclones in the Eratosthenes region also tend to be very differentiated from their neighbors. Figure 8b classifies anticyclones in terms of mean maximal speed radius as a function of lifetime; each dot is an anticyclone labelled as *order 0* for the 7 regions studied in Fig. 6, with red color highlighting Eratosthenes anticyclones. The background is a density probability plot for all anticyclones in the LB - except Eratosthenes anticyclones to enhance comparison. The scatter plot presents an overall spread, with maximal density between 15 and 25 km, consistent with the limit of altimetric resolution (1/8 °). However long-lived Eratosthenes anticyclones form a clear cluster of eddies living longer than a year with a radius often greater than 40 km, outside the 90% probability contour. Not all Eratosthenes anticyclones are encompassed in this category, because the *order 0* label also encompasses some short-lived eddies quickly merging, which therefore unlikely have unusual characteristics, hence the some red dots being also scattered. Eratosthenes anticyclones are the only eddies in the southeastern part of the LB presenting such dynamical characteristics: apart from 2 outliers, this is the only region where the maximal speed radius can exceed 40 km, more than three time the internal deformation radius of approximately 10 to 12 km in the Mediterranean sea (Mkhinini et al., 2014). This suggests the existence of differentiation mechanisms acting on the eddy lifetime and radius.

4.4 Anticyclones detachments from the Levantine coast

In Sect. 4.3 the Eratosthenes attraction basin was identified, notably attracting anticyclones originally formed near the Levantine coast as seen in altimetric tracks (see Fig. 6a). Altimetric eddy detections have however important limitations stemming from the large spatio-temporal interpolation between satellite measurement tracks. This makes the resolution of altimetric maps (1/8° in the Mediterranean sea) not sufficient to adequately detect small-scale structures and introduces uncertainty in the detection, especially as the internal deformation radius is small (Le Vu et al., 2018). Nevertheless, other sources of satellite images such as SST contain visible eddy signatures on them (Moschos et al., 2020). On such images, we can observe filament exchanges between eddies as well as eddies moving too fast to be detected through altimetry, as are eddies detaching from the Levantine coast. Gertman et al. (2010) already spotted such a detachment in August 2009 by means of in situ data of drifting buoys. Here, we provide observational evidence through SST images of a similar event occurring on July 2016 where a detached warm-core anticyclonic ring, part of cyclone-anticyclone dipole, will rapidly merge with another anticyclonic eddy which will later merge with the Eratosthenes anticyclone. Figure 9 portrays this event through four daily SST image snapshots where the altimetric detection DYNED contours have been superimposed. An anticyclone not detected by surface altimetry with a particularly warm surface signature can be spotted on the right-hand side of Fig. 9a (17/07/2016). A cyclone with which it forms a dipole can be seen on the SST in its south-east corner, and is also detected by the altimetry somewhat more southwards. Five days later in panel 9b (22/07/2016) this anticyclone has moved rapidly towards the DYNED anticyclone #10754, first detected on 10/02/2016, offshore Haifa. The track of DYNED anticyclone #10754 is depicted with a blue line. The warm-core detached anticyclone will eventually merge with it 6 days later, in 9c (28/07/2016). A month later, in panel 9d (02/09/2016), this anticyclone will eventually merge with the eddy on the Eratosthenes seamount, having transferred the warm waters and the momentum of the detached warm-core eddy.

4.5 Mersa-Matruh attractor

Eddy attraction to the other big anticyclonic structure of the region, called "Mersa-Matruh", can be studied in comparison to the Eratosthenes attractor. In Fig. 10 the Lagrangian framework defined in Sect. 3.1 is applied to this region. Firstly, it is notable that this structure clearly also acts as an attractor, the total number of *importing* eddy (sum of *order 0-1-2*) being a lot higher than *order 0* alone and *exporting* eddies. In a similar fashion with the Eratosthenes region, which acts as a stranding place for anticyclones detached from the Levantine coast, lots of anticyclones detached from the Libyo-Egyptian coast (likely as instability of the Libyo-Egyptian current) end into the Mersa-Matruh, often trough one merging or more. In particular a hotspot of anticyclone formation takes place in the Mersa-Matruh gulf approximately at (31.5° N , 27.5° E) from which 5 anticyclones drifted towards the Mersa-Matruh structure. No importing anticyclones come from the north, as expected given that almost no anticyclones occur in the Rhodes gyre (see Fig. 4a).

However in contrast to the Eratosthenes attraction basin being isolated with very few anticyclone exchanges outside, the Mersa-Matruh anticyclone has no clear western boundaries. For instance some merging export trajectories in red are present southwestwards, pointing out that some eddies escaped from this structure. On the contrary, one Ierapetra eddy did end through successive mergings into the Mersa-Matruh area. This individual event seems to be isolated, as shown in Ioannou et al. (2017), Ierapetra eddies actually tend to go westwards riding up the Libyo-Egyptian current if they move away, in a similar way to the eddy behaviour described by Sutyrin et al. (2009). More generally, the importance of *higher order* anticyclones merging in successive steps to Mersah-Matruh anticyclone suggests that convergence is less straightforward and clear than for the EAA, likely because topographic constraints are less present.

5 Vertical structure of the Eratosthenes anticyclone attractor

The DYNED-Altas colocalisation and background method (see Sect. 3.3) is used to estimate the heat, salt and density anomalies associated with each eddy. For very persistent long-lived eddies, such as those constituting the EAA, this allows to observe changes in the vertical structure and the evolution of the associated anomalies. Figure 11 shows for different years during the 2000-2018 period the annual averaged vertical profiles of the Eratosthenes attractor, over all available profiles within each year, and closer than 30 km to the eddy center. A histogram below indicates for each year how many profiles are available. This number varies a lot due to inconstant frequency of oceanographic surveys, with years 2008 to 2011 being over-represented because of extensive glider sections (Hayes et al., 2011) and several Argo floats being trapped for a very long time inside the anticyclone.

In the annual averaged vertical profiles in Fig. 11, the EAA anticyclones can be characterized by very deep anomalies, both in salt and temperature. For every year the depth of maximal density anomaly is below 200 m and reaches some years 450 m. Magnitude of the anomalies can also be extremely marked, higher than 2.5°C and 0.45 PSU in 2010. However, if annually averaged temperature anomalies always reach 1°C at 200 m or below, Fig. 11 especially shows that there is a strong interan-

nual variability in the vertical structures of these anticyclones. 2010 then appear as an extreme event, with the formation of a double-core structure visible on the density profile (Fig. 12c). This event was surveyed by gliders and described by Hayes et al. (2011), but here with longer timeseries it can be seen that eddy-induced anomalies in 2009-2010 were extreme compared to the 19 years mean vertical structure.

Moutin and Prieur (2012) also compared in the BOUM campaign in 2008 the vertical structure of an Eratosthenes anticyclone with 2 others anticyclones in the Mediterranean sea: a detached Algerian eddy and an anticyclone in the central Ionian sea. Their comparison showed that the anticyclone constituting the EAA had the deepest potential density maximal anomaly, at 380 m compared to 160 m in the Algerian eddy, and that integrated anomalies were very warm and salty waters, with temperature and salinity anomalies of $+2.35$°C and $+0.388$ PSU (respectively $+0.75$°C and -0.65 PSU in the Algerian eddy). Such values are consistent with observations in other years as shown in Fig. 11b-c, although slightly higher.

The vertical structure of Eratosthenes anticyclones described above should be compared with physical properties of neighbouring eddies in the LB. Figure 12 presents the comparison between a section representative of the Eratosthenes anticyclone, using data from the BOUM campaign in June 2008 (Moutin and Prieur, 2012), and an anticyclone section in the Tel-Aviv region performed in October 2018 by a glider from IOLR. Next to each section is an ADT map representative of the SSH activity at that time (panels b and d). The glider section lasts for 10 days, 20th of October 2018 being the median date and a magenta line indicates the glider track, on which the position on the 20th of October is shown with a magenta circle. On the ADT maps the daily altimetric eddy contours are plotted, with cyclones in red and anticyclones in blue, and a dot with size proportional to the vortex Rossby number indicates the center. The upper panel of each section (panels 12a and 12c) marks with a blue line the part of the cross-section which is inside the maximal speed anticyclone contour. Thin black lines in the vertical sections are the absolute temperature isotherms, whereas the color indicates the temperature anomaly relative to the climatological background; isotherms interval and colorbar range are the same in both sections for comparison purpose. An important difference is that panel 12a is an interpolation between the CTD measurements (indicated by black crosses) whereas panel 12b shows a glider track stacking of which each pixel corresponds to a measurement.

Although a 10-years period separates the two sections, it should first be noted that the local eddy activity is similar in both events, and very close to the mean circulation deduced from Fig. 1: anticyclones are found in Eratosthenes, Herodotus, and Tel-Aviv regions, whereas a cyclone is found in the Haifa region. Furthermore as can be seen in the ADT maps, both sections crossed the anticyclones close to their respective center, allowing to assume that the maximal anomaly was adequately sampled. Extensive gliders sections were surveyed in the Eratosthenes region in 2009 and 2010, but as explained above, 2010 appears as an extreme year where comparison with neighbouring eddies will be biased.

The anticyclone constituting the EAA surveyed in Fig. 12a is a long-lived anticyclone, referenced in the DYNED database with number #4914, born in the Beyrut region before settling over the Eratosthenes seamount for more than 6 months. The

"Tel-Aviv" eddy measured in Fig. 12c is a young anticyclone, formed close to the shore in August 2018 as detected by AMEDA, at the approximate position 32.0° N, 34.0° E, and referenced as DYNED #12683. It drifted slowly offshore northwestwards before dying without merging at approximately 32.5° N, 33.0° E at the beginning of December 2018. It is therefore very similar to the anticyclones formed in the Tel-Aviv region and drifting offshore, sometimes achieving to merge in the Eratosthenes region, in a similar way to the trajectories shown in Fig. 6c. In both events the "Tel-Aviv" anticyclone appears to be more intense in terms of Rossby number than the "Eratosthenes" one (as shown by a larger dot on the ADT maps), but the vertical structure shows that the Eratosthenes anticyclone, although weak in altimetric signature, hides a very deep and strong temperature anomaly: +2.35°C at 380 m compared to +1.3°C at a depth of maximal density anomaly of 250 m in the "Tel-Aviv" anticyclone. This comparison shows that anticyclones in the EAA are also differentiated from neighbouring eddies by a deeper subsurface anomaly, consistent with first observations by Stegner et al. (2019) showing that depth of maximal density anomaly over the Eratosthenes seamount often below 300 m are an almost unique specificity in the whole Mediterranean sea.

6 Discussion

Hamad et al. (2006) showed with only three years of SST data that along-shore current instabilities create eddies drifting offshore, already identifying the Eratosthenes seamount as an anticyclone accumulation area (see their Fig. 16). With the hindsight of 19 years of eddy tracking, we add in this study a quantification of the *importing* eddy flux and confirmed what was previously inferred through a limited time period of data. We also observe that anticyclones are actually often formed offshore close to the seamount on the west, in the region called in this study "Herodotus".

Another important result of the eddy tracking performed here is the isolation of anticyclone dynamics from the rest of the LB: almost no anticyclones come from areas further west than the Herodotus region, and conversely almost none escape this attraction basin (dashed black line on Fig. 3, 4, 6a-g and 7). It can be noted in Fig. 4a that the dashed line coincides with anticyclone drift divergence. This observation is not true for cyclones, but as they do not have a thick core of homogeneous water and live significantly shorter than anticyclones (see Fig. 5), they are assumed to contribute less to water mass transport. This western impermeable border could be linked to the presence of the Middle-Mediterranean Jet (MMJ). Zodiatis et al. (2010) suggested this jet could be feeding the Eratosthenes anticyclonic structure. Nevertheless, the jet could also act as a barrier for anticyclone, explaining the absence of anticyclone flux from the Mersa-Matruh area into the Eratosthenes region (see Fig. 6a).

In older literature, Robinson et al. (1991) discussed the hypothesis of a northern path of Atlantic waters in the LB, isolating its south-eastern part, but grouping together the Mersa-Matruh and Eratosthenes structures. This analysis was performed with a hydrographic vision using CTD stations. More recently Ayata et al. (2018) did a review of the Mediterranean regionalisation across 8 studies using various parameters, but mainly with a biological or hydrological focus. A remarkable result from this review is a very good agreement of these studies on distinguishing a region of homogeneous properties in the Southeastern LB,

called "Levantine". The region proposed by the authors (see Fig. 4 in in Ayata et al. (2018)) matches very well the borders of the EAA attraction basin delineated by this study, apart from the edge along the Egyptian and Levantine coasts. These results thus suggest a real hydrographic significance of the EAA attraction basin and a possible role of anticyclones in homogenizing water masses properties.

Additionally given the importance of this area for intermediate water formation, the fate of watermasses in the EAA core and its dissipation would be of great interest for extended research. Anticyclones coming from different formation areas regularly merge with the EAA, and the imported water masses should therefore be transported. They likely feed its subsurface anomaly, which was shown to be deeper than surrounding structures (see Fig. 12), but later the final destination of these waters is unknown. Erosion from its deep anomaly due to intense shear due to topographic interaction with a seamount (Sutyrin et al., 2011) could give a warm and salty water flux in depth and leading to intermediate waters formation. Answering this very important question requires further simulation work, but also more in-situ oceanographic data forming a consistent and continuous three-dimensional time series to accurately follow its evolution.

This study reveals the existence of the EAA from analysis of eddy tracks, but questions remain regarding the mechanisms explaining this anticyclone convergence, whereas more classical westwards β-drift (Chelton et al., 2011) or current advection along the coast (Sutyrin et al., 2009) could be expected. There is controversy on whether the EAA effectively attracts other eddies, or conversely if eddies detach from the coast and merge with a central and long-lived structure. In other words does the EAA pull other anticyclones towards the seamount (an active way) or is it acting as the stranding point of anticyclones advected by the mean flow (a passive way) ? SST images and detachments observed from the coast, shown in Fig. 9 in this study but previously observed in the literature by Hamad et al. (2006) and Gertman et al. (2010), suggest the second option is likely happening. On the other hand the high occurrence of eddy merging and splitting highlights the importance of eddy-to-eddy interaction in this basin. Further studies in this direction are needed to outline eddy dynamics, reminding that the small internal deformation radius in the Mediterranean sea of 10 to 12 km (Mkhinini et al., 2014) allows to accurately detect only large mesoscale structures. Nevertheless, great improvements are possible by applying eddy automatic detection at smaller scales than the mesoscale with the help of SST data (Moschos et al., 2020).

The presence of the EAA over a seamount obviously raises the question of topographic interactions. Two attractors structures are observed in the LB, over very different bathymetry: the Mersa-Matruh attractor over the Herodotus trench deeper than 2000 m and the EAA over the Eratosthenes seamount whose summit is approximately 700 m deep. This similarity suggests that interactions with the seamount do not play a significant role in anticyclone convergence towards the EAA, and actually if significant the presence of a seamount should rather destabilize anticyclone dynamics (Sutyrin et al., 2011). However some differences between these structures (see Sect. 4.5), notably the more variable average position or attraction basin of Mersa-Matruh, could be explained by topographic interactions.

Last but not least, the background used to estimate eddy vertical structure in Sect. 5, is considered a climatological reference at the same approximate location and time of the year (see Sect. 3.3). However it is computed as a 2000-2018 average and could then be altered by events of strong interannual variability, reported in the LB by Ozer et al. (2017). Long-term evolution of eddy-induced physical property signature would deserve further work.

7   Conclusions

Using the DYNED-Atlas of eddies in the Mediterranean sea, a Lagrangian convergence method is defined, and its application to anticyclone tracking from 2000 to 2018 enables to quantify anticyclone transfers between sub-regions of the Southeastern LB. At the position of a known area of anticyclone accumulation, it reveals the existence of anticyclone convergence toward the Eratosthenes seamount in a structure we named *Eratosthenes anticyclone attractor*. This attractor proves not to be a single fixed anticyclone but being constituted by the succession of long-lived anticyclones sharing dynamical characteristics, distinct from neighbouring eddies: longer lifetime - more than a year and up to 4 years - and a maximal speed radius above 40 km - more than three times the internal deformation radius. Lagrangian eddy tracking also showed that the convergence towards the EAA is geographically bounded to a clear *attraction basin*. Anticyclones drift towards the Eratosthenes seamount after detaching from the current along the Levantine coast or being formed westward in the region we named "Herodotus". Formation of anticyclones with short lifetime quickly merging with EAA are spotted in the regions called "Tel-Aviv" and "Haifa". An effective barrier for anticyclones is then found between the Eratosthenes and Mersa-Matruh regions. In situ vertical profiles are colocalized with eddies and climatological backgrounds are computed using the DYNED-Atlas method, allowing to estimate the eddy-induced physical property signatures. The anomalies induced by the anticyclones constituting the EAA are found to be extremely deep, with depths of maximal density anomaly always at or below 200 m, reaching some years 450 m, but with pronounced interannual variability. Annual averages of temperature anomaly are found to be always equal or greater than $+1°C$ at 300 m, revealing a large heat storage capacity of the anticyclone.

Author contributions. A. Barboni did the main analysis and wrote the manuscript; A. Lazar supervised the study and provided the glider data; A. Stegner supervised the study; E. Moschos analyzed SST data and produced Fig. 9. All authors contributed to finalize the manuscript.

Competing interests. The authors declare that they have no conflict of interest.

Acknowledgements. This research was supported by THE ISRAEL SCIENCE FOUNDATION (grant No. 1666/18)

References

485 Amitai, Y., Lehahn, Y., Lazar, A., and Heifetz, E.: Surface circulation of the eastern Mediterranean Levantine basin: Insights from analyzing 14 years of satellite altimetry data, Journal of Geophysical Research: Oceans, 115, 2010.

ARGO: Argo float data and metadata from Global Data Assembly Centre (Argo GDAC), https://doi.org/10.17882/42182, https://www.seanoe.org/data/00311/42182/, 2020.

Ayata, S.-D., Irisson, J.-O., Aubert, A., Berline, L., Dutay, J.-C., Mayot, N., Nieblas, A.-E., d'Ortenzio, F., Palmiéri, J., Reygondeau, G.,
490 et al.: Regionalisation of the Mediterranean basin, a MERMEX synthesis, Progress in Oceanography, 163, 7–20, 2018.

Brenner, S.: Long-term evolution and dynamics of a persistent warm core eddy in the Eastern Mediterranean Sea, Deep Sea Research Part II: Topical Studies in Oceanography, 40, 1193–1206, 1993.

Chelton, D. B., Schlax, M. G., and Samelson, R. M.: Global observations of nonlinear mesoscale eddies, Progress in oceanography, 91, 167–216, 2011.

495 Cui, W., Wang, W., Zhang, J., and Yang, J.: Multicore structures and the splitting and merging of eddies in global oceans from satellite altimeter data, Ocean Science, 15, 413–430, 2019.

de Marez, C., L'Hégaret, P., Morvan, M., and Carton, X.: On the 3D structure of eddies in the Arabian Sea, Deep Sea Research Part I: Oceanographic Research Papers, 150, 103 057, 2019.

DYNED-Atlas-Med: Stegner, A. and Le Vu, B. and Pegliasco, C. and Faugere, Y. Dynamical Eddy Atlas of the Mediterranean-Sea 2000-
500 2018. MISTRALS: https://doi.org/10.14768/2019130201.2, 2019.

Garreau, P., Dumas, F., Louazel, S., Stegner, A., and Le Vu, B.: High-Resolution Observations and Tracking of a Dual-Core Anticyclonic Eddy in the Algerian Basin, Journal of Geophysical Research: Oceans, 123, 9320–9339, 2018.

GEBCO: GEBCO Compilation Group (2020) GEBCO 2020 Grid (doi:10.5285/a29c5465-b138-234d-e053-6c86abc040b9), 2020.

Gertman, I., Goldman, R., Rosentraub, Z., Ozer, T., Zodiatis, G., Hayes, D., and Poulain, P.: Generation of Shikmona anticyclonic eddy from
505 an alongshore current, in: Rapp. Comm. int. Mer Medit.(CIESM Congress Proceedings), vol. 39, p. 114, 2010.

Hamad, N., Millot, C., and Taupier-Letage, I.: The surface circulation in the eastern basin of the Mediterranean Sea, Scientia Marina, 70, 457–503, 2006.

Hayes, D., Zodiatis, G., Konnaris, G., Hannides, A., Solovyov, D., and Testor, P.: Glider transects in the Levantine Sea: Characteristics of the warm core Cyprus eddy, in: OCEANS 2011 IEEE-Spain, pp. 1–9, IEEE, 2011.

510 Ioannou, A., Stegner, A., Le Vu, B., Taupier-Letage, I., and Speich, S.: Dynamical evolution of intense Ierapetra eddies on a 22 year long period, Journal of Geophysical Research: Oceans, 122, 9276–9298, 2017.

Ioannou, A., Stegner, A., Tuel, A., Levu, B., Dumas, F., and Speich, S.: Cyclostrophic corrections of AVISO/DUACS surface velocities and its application to mesoscale eddies in the Mediterranean Sea, Journal of Geophysical Research: Oceans, 2019.

Laxenaire, R., Speich, S., Blanke, B., Chaigneau, A., Pegliasco, C., and Stegner, A.: Anticyclonic eddies connecting the western boundaries
515 of Indian and Atlantic Oceans, Journal of Geophysical Research: Oceans, 123, 7651–7677, 2018.

Laxenaire, R., Speich, S., and Stegner, A.: Evolution of the Thermohaline Structure of One Agulhas Ring Reconstructed from Satellite Altimetry and Argo Floats, Journal of Geophysical Research: Oceans, 2019.

Le Vu, B., Stegner, A., and Arsouze, T.: Angular Momentum Eddy Detection and tracking Algorithm (AMEDA) and its application to coastal eddy formation, Journal of Atmospheric and Oceanic Technology, 35, 739–762, 2018.

520 Mason, E., Pascual, A., and McWilliams, J. C.: A new sea surface height–based code for oceanic mesoscale eddy tracking, Journal of Atmospheric and Oceanic Technology, 31, 1181–1188, 2014.

Mason, E., Ruiz, S., Bourdalle-Badie, R., Reffray, G., García-Sotillo, M., and Pascual, A.: New insight into 3-D mesoscale eddy properties from CMEMS operational models in the western Mediterranean, 2019.

Matsuoka, D., Araki, F., Inoue, Y., and Sasaki, H.: A new approach to ocean eddy detection, tracking, and event visualization–application to
525 the northwest pacific ocean, Procedia Computer Science, 80, 1601–1611, 2016.

Menna, M., Poulain, P.-M., Zodiatis, G., and Gertman, I.: On the surface circulation of the Levantine sub-basin derived from Lagrangian drifters and satellite altimetry data, Deep Sea Research Part I: Oceanographic Research Papers, 65, 46–58, 2012.

Millot, C. and Taupier-Letage, I.: Circulation in the Mediterranean sea, in: The Mediterranean Sea, pp. 29–66, Springer, 2005.

Mkhinini, N., Coimbra, A. L. S., Stegner, A., Arsouze, T., Taupier-Letage, I., and Béranger, K.: Long-lived mesoscale eddies in the eastern
530 Mediterranean Sea: Analysis of 20 years of AVISO geostrophic velocities, Journal of Geophysical Research: Oceans, 119, 8603–8626, 2014.

Moschos, E., Stegner, A., Schwander, O., and Gallinari, P.: Classification of Eddy Sea Surface Temperature Signatures under Cloud Coverage, IEEE Journal of Selected Topics in Applied Earth Observations and Remote Sensing, 2020.

Moutin, T. and Prieur, L.: Influence of anticyclonic eddies on the Biogeochemistry from the Oligotrophic to the Ultraoligotrophic Mediter-
535 ranean (BOUM cruise), Biogeosciences, 9, 3827–3855, 2012.

Ozer, T., Gertman, I., Kress, N., Silverman, J., and Herut, B.: Interannual thermohaline (1979–2014) and nutrient (2002–2014) dynamics in the Levantine surface and intermediate water masses, SE Mediterranean Sea, Global and Planetary Change, 151, 60–67, 2017.

Pessini, F., Olita, A., Cotroneo, Y., and Perilli, A.: Mesoscale eddies in the Algerian Basin: do they differ as a function of their formation site?, Ocean Science, 14, 2018.

540 Robinson, A., Golnaraghi, M., Leslie, W., Artegiani, A., Hecht, A., Lazzoni, E., Michelato, A., Sansone, E., Theocharis, A., and Ünlüata, Ü.: The eastern Mediterranean general circulation: features, structure and variability, Dynamics of Atmospheres and Oceans, 15, 215–240, 1991.

Stegner, A., Le Vu, B., Pegliasco, C., Moschos, E., and Faugere, Y.: 3D structure of long-lived eddies in the Mediterranean sea : the DYNED-Atlas database, Rapport Commission internationale Mer Méditerranée, 42, 2019.

545 Sutyrin, G., Stegner, A., Taupier-Letage, I., and Teinturier, S.: Amplification of a surface-intensified eddy drift along a steep shelf in the Eastern Mediterranean Sea, Journal of physical oceanography, 39, 1729–1741, 2009.

Sutyrin, G., Herbette, S., and Carton, X.: Deformation and splitting of baroclinic eddies encountering a tall seamount, Geophysical & Astrophysical Fluid Dynamics, 105, 478–505, 2011.

Taburet, G., Sanchez-Roman, A., Ballarotta, M., Pujol, M.-I., Legeais, J.-F., Fournier, F., Faugere, Y., and Dibarboure, G.: DUACS DT2018:
550 25 years of reprocessed sea level altimetry products, Ocean Science, EGU, 2019.

Yi, J., Du, Y., He, Z., and Zhou, C.: Enhancing the accuracy of automatic eddy detection and the capability of recognizing the multi-core structures from maps of sea level anomaly, Ocean Science, 10, 39–48, 2014.

Zodiatis, G., Hayes, D., Gertman, I., and Samuel-Rhodes, Y.: The Cyprus warm eddy and the Atlantic water during the CYBO cruises (1995-2009), Rapp. Comm. Intern. Mer Mediter, 39, 202, 2010.
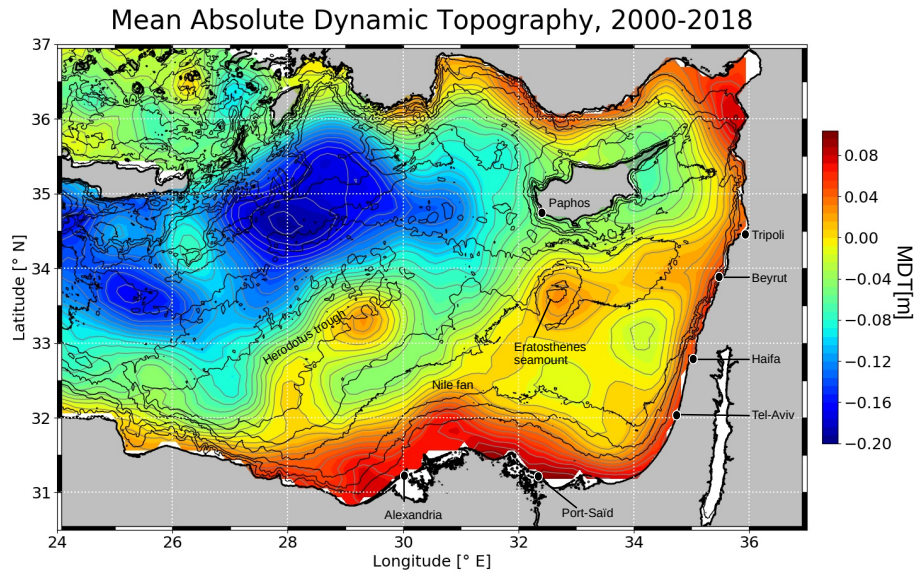
Figure 1. MDT map of the LB and several toponyms and city names used in this study. Thin black lines are the -100, -500, -1000, -1500, -2000 and -2500 m isobaths, thick black line is the 0 m isobath. Bathymetry is retrieved from GEBCO (2020). The same isobaths are shown on all maps.
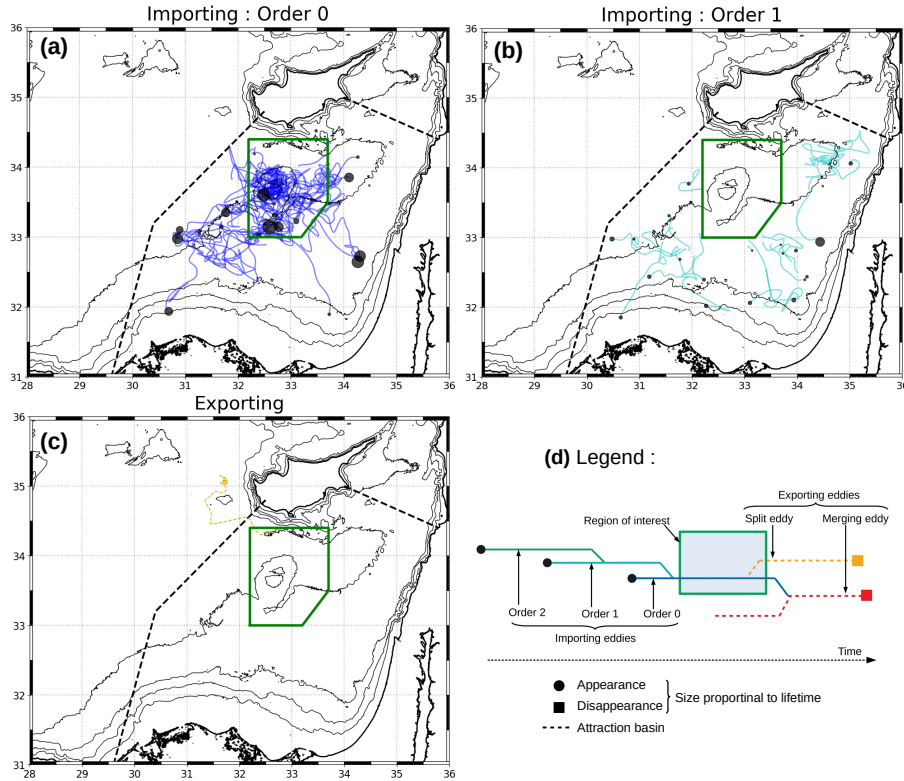
Figure 2. Lagrangian convergence framework applied to anticyclones in the Eratosthenes seamount region and detailed in several steps. (a) *Order 0*: eddies converging directly; (b) *Order 1*: eddies merging with an *order 0* eddy; (c) *Exporting split* and *merging* eddies (no cases of the latter detected here). Locations of eddy appearance for (a) and (b) (respectively disappearance for (c)) are shown with black dots (respectively colored squares) whose size is proportional to the eddy lifetime. (d) Legend. Black dashed line is the attraction basin introduced in Sect. 4.3.
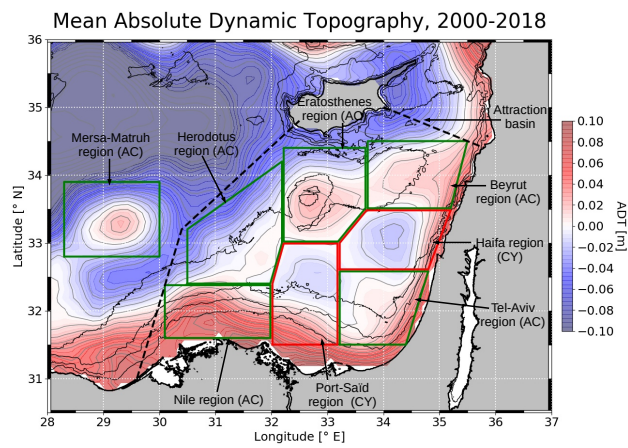
Figure 3. MDT map of the Southeastern LB labelled with borders and names of the studied regions. Anticyclonic regions (AC) have a green border, cyclonic regions (CY) a red one, boxes coordinates being indicated in appendix (Table A1). ~~B lack~~ Black dashed line is the attraction basin introduced in Sect. 4.3.
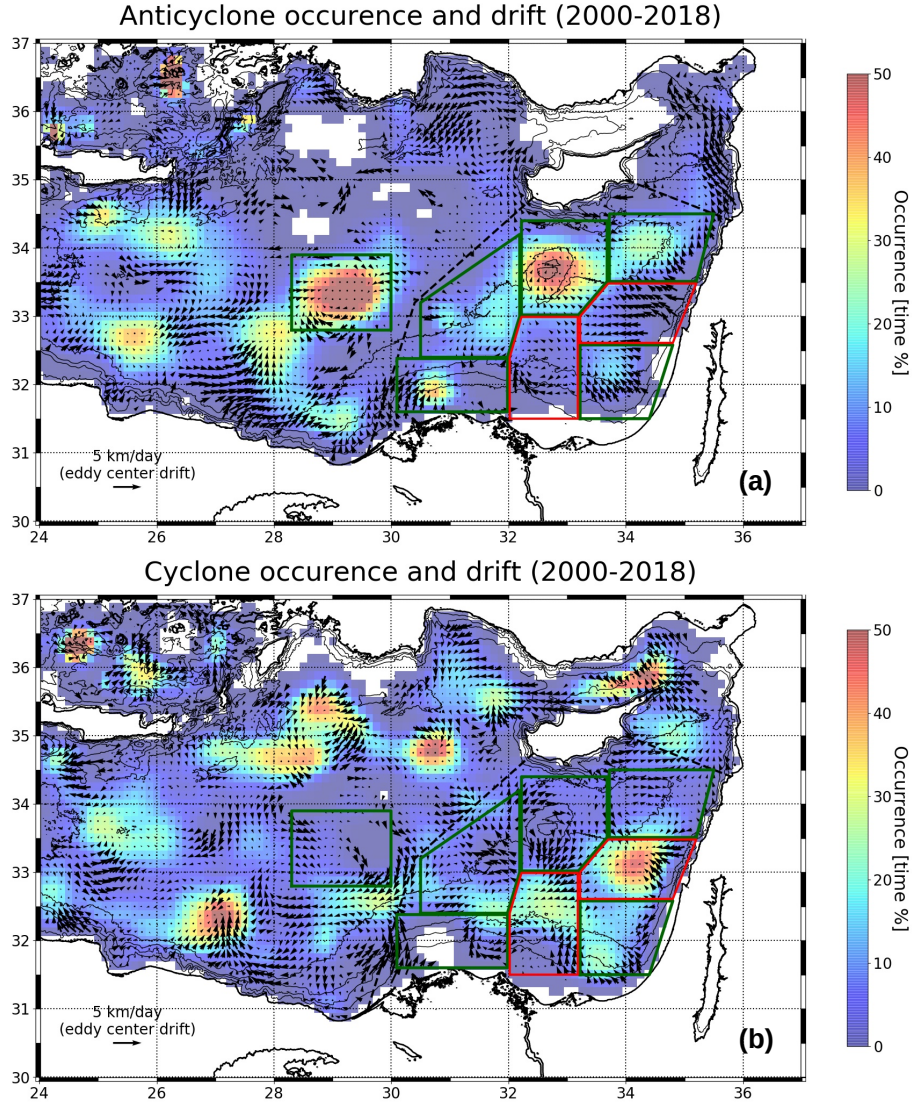
Figure 4. Eddy occurrence and drift in the LB for (a) anticyclone and (b) cyclones. Pixel size is (1/8°x 1/8°). Occurrence is shown as the time percentage when the pixel center spends inside maximal speed contours of eddies. Eddy drift is the mean Lagrangian drift of the eddy centers on pixels where more than 5 eddy centers passed, with Gaussian smoothing (kernel size (5x5)). AC (resp. CY) regions defined in Sect. 3.2 are drawn with a green (red) solid line, attraction basin defined in Sect. 4.3 with a black dashed line.
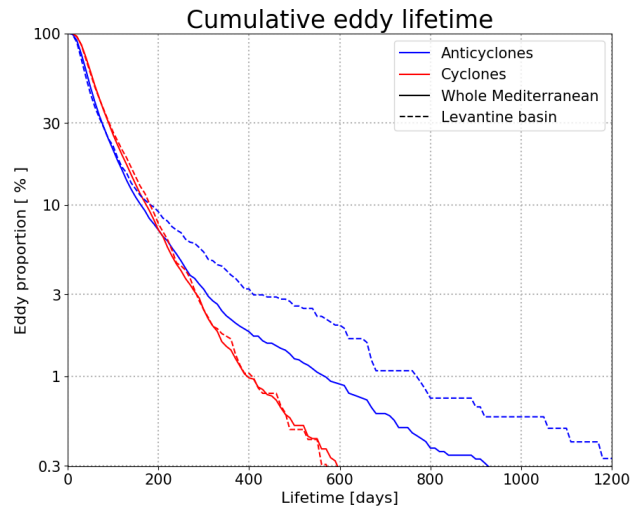
Figure 5. Cumulative eddy lifetime as percentage in logarithmic scale, separated for cyclones and anticyclones and for the LB and the whole Mediterranean sea.
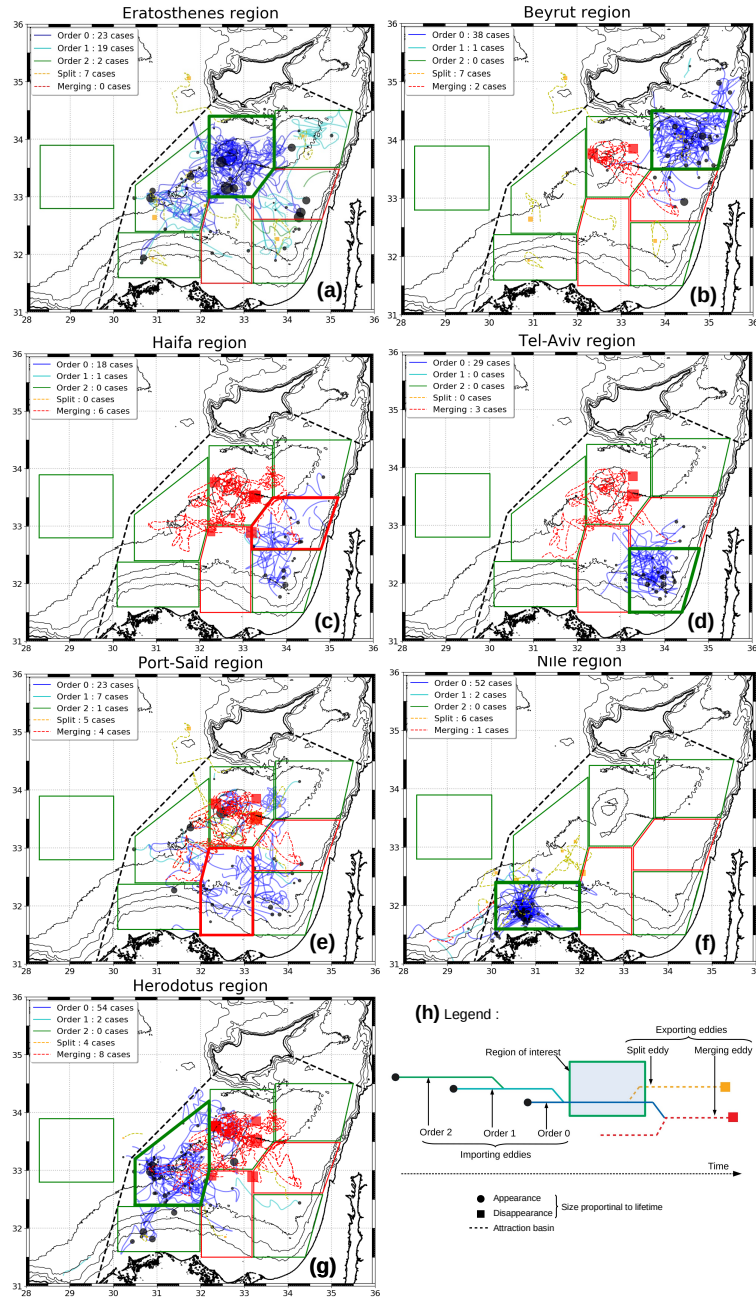
Figure 6. Eddy exchanges framework applied to (a) Eratosthenes, (b) Beyrut, (b) Haifa, (d) Tel-Aviv, (e) Port-Saïd, (f) Nile and (g) Herodotus region. For each panel all other regions are shown (green borders for AC regions, red borders for CY ones), while a thicker line indicates the studied region. Color chart used is summarized in panel (h). Mersa-Matruh region is studied later in Fig. 10.
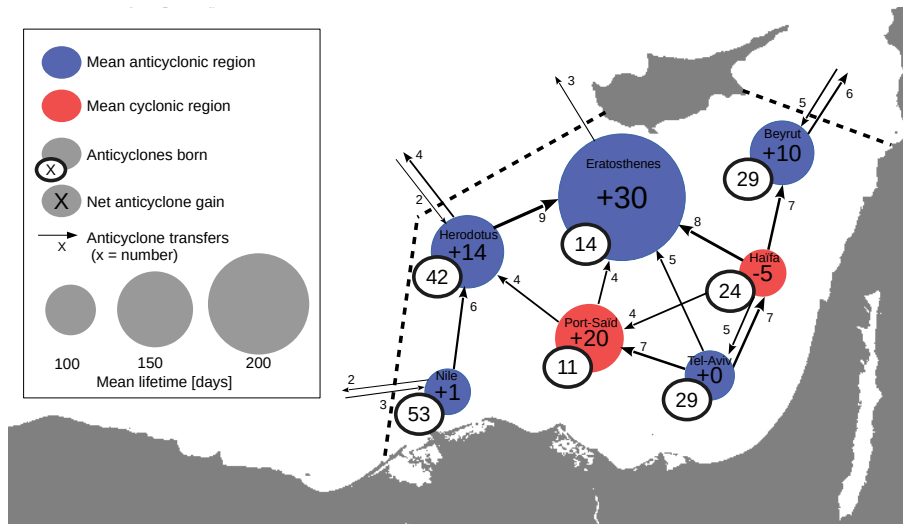
Figure 7. Scheme summarizing inter-region anticyclone transfers within the EAA attraction basin (dashed line). Transfers encompass *order 0-1-2* anticyclones. Within this basin, only transfers higher or equal to 4 are represented by arrows, for readability purpose. Across the basin border all transfers are shown. Arrow thickness is proportional to eddy transfers. Red circles represent CY regions, blue circles AC ones, with radius proportional to anticyclone mean lifetime in the region. All details are resumed in Table A2 in appendix.
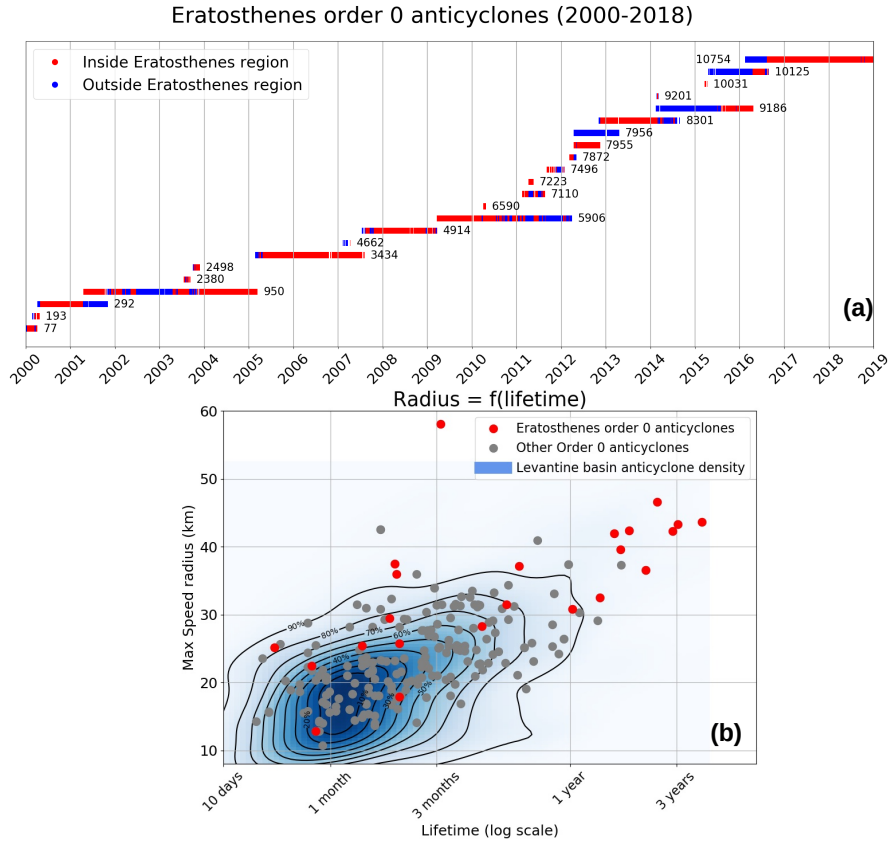
Figure 8. Detail of the anticyclones constituting the EAA, detected as *order 0* for the Eratosthenes region (tracks in Fig. 2a). (a): Timeseries with eddy ID number from the DYNED database. The color marker indicates when the eddy center is within (red) or outside (blue) the region. (b): Scatter plot of maximum speed radius as a function of lifetime, in logarithmic scale, for *order 0* anticyclones of the Eratosthenes region (red dots) and the other regions (gray dots); blue shaded background is the density function for the whole LB anticyclones - except Eratosthenes ones - with contours each 10% probability step.
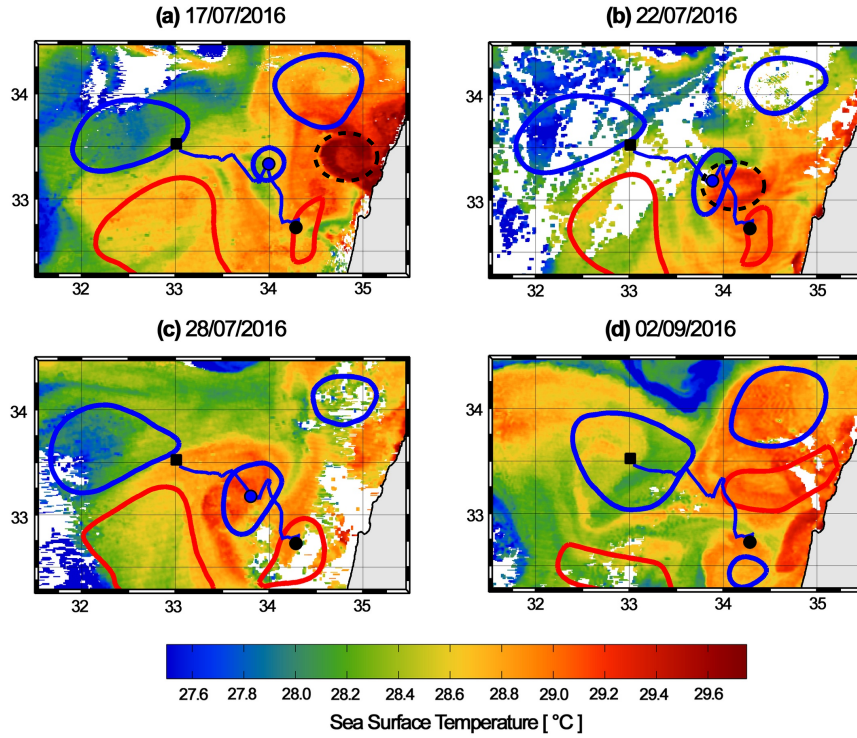
Figure 9. Daily snapshots of SST images showing a quickly moving warm-core anticyclone, part of a dipole, which detaches from the Levantine coast and merges with a future Eratosthenes anticyclone. Superimposed DYNED contours are blue for anticyclones and red for cyclones. The track of the studied anticyclone is in blue line, its current center with a blue circle, its initial detection on 10/02/2016 with a black circle and its last detection on 02/09/2016 with a black square. A blue line approximates the track of the warm-core anticyclone as seen in the SST sequence.
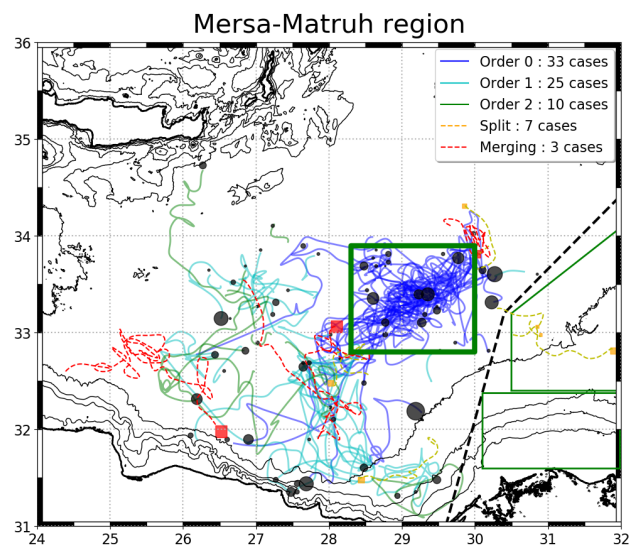
Figure 10. Convergence structure applied for the Mersa-Matruh region, in the same way and same color code as in figure 6.
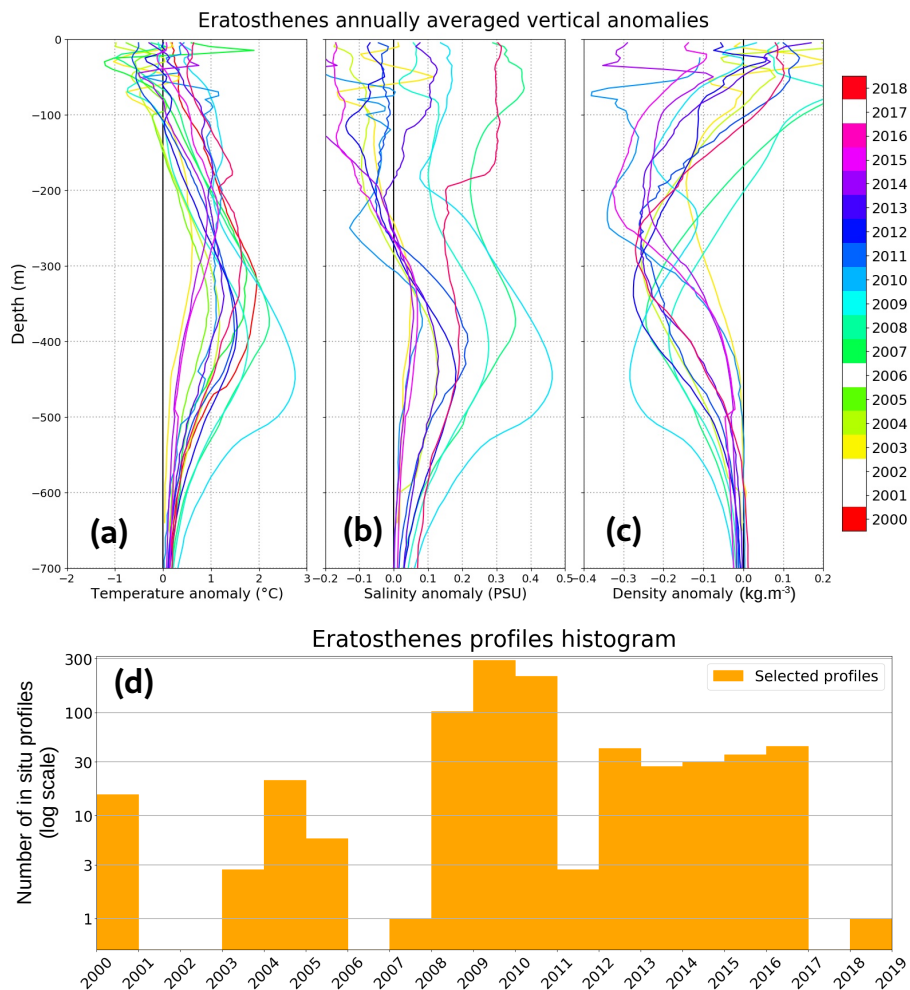
Figure 11. For each year, average of the vertical profiles anomalies, for (a) in situ temperature, (b) salinity and (c) density, inside Eratosthenes *order 0* anticyclones. Profiles are selected if they are cast within 30 km from the eddy center and their histogram is shown in panel d, with a log scale. Years without any profiles are discarded from the colorbar. Some years (e.g. 2005) present only a temperature profile as only XBT casts were available.
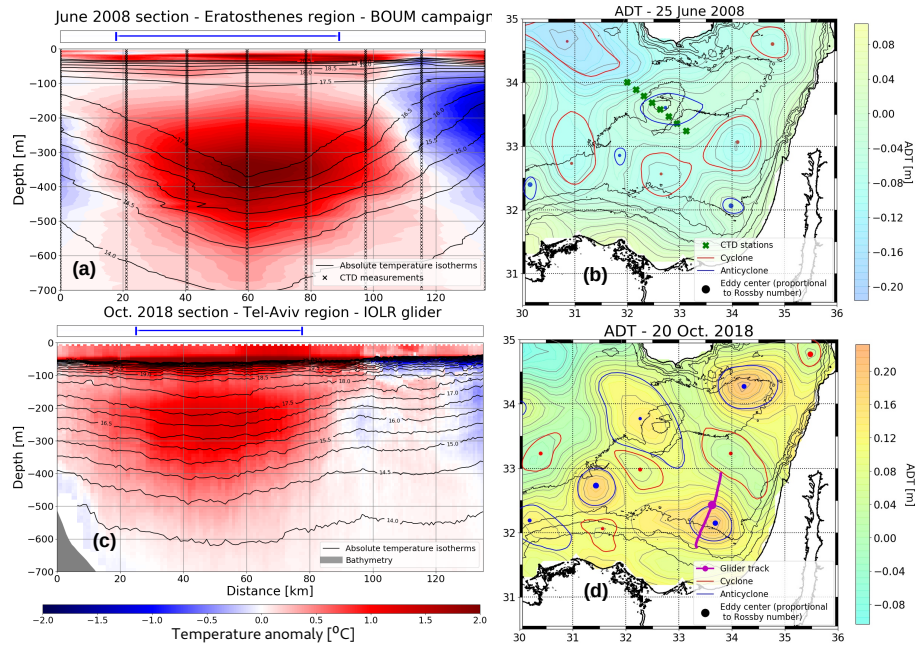
Figure 12. Comparison of anticyclone sections. Left panel (a) (respectively (c)): Eratosthenes (Tel-Aviv) region anticyclone section in June 2008 (mid-October 2018); north on the left side; horizontal axis (shared) is distance along the section; black lines are absolute temperature isotherms and the temperature anomaly as color background; blue cartridge above the panel reminds maximal speed limits. Right panel (b) (respectively (d)): ADT map presenting the eddy neighbouring eddy activity, green crosses (a magenta line) showing the CTD casts (the glider track); eddy contours are maximal speed contours, blue for anticyclones, red for cyclones, with a Rossby number-scaled dot for its center.

555   ~~Cyclone transfers for Haifa region. Same as Fig. 6c but with Lagrangian convergence framework applied to cyclones. Boxes and dashed line are the same as in Fig. 3.~~
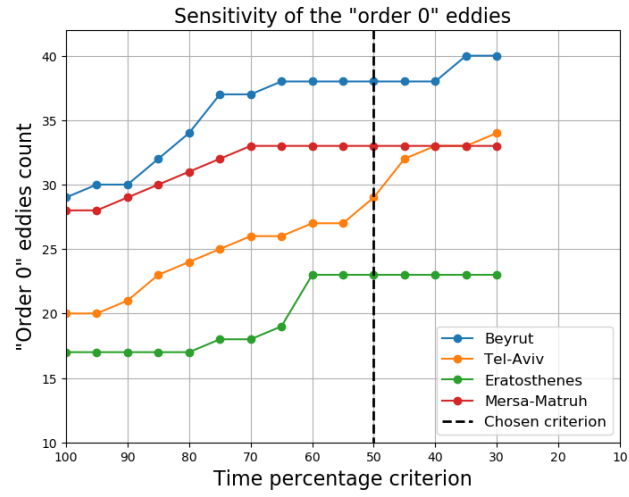
Figure A1. Sensitivity of the total number of *order 0* anticyclones with the lifetime criterion, for 4 chosen regions. "100%" means *order 0* anticyclones are strictly and only the ones dying in the studied region, "30%" means that *order 0* are the ones dying in the studied region, plus the ones spending 30% of their lifetime within the borders of this region. 50% is chosen in this study, see Tab A2.
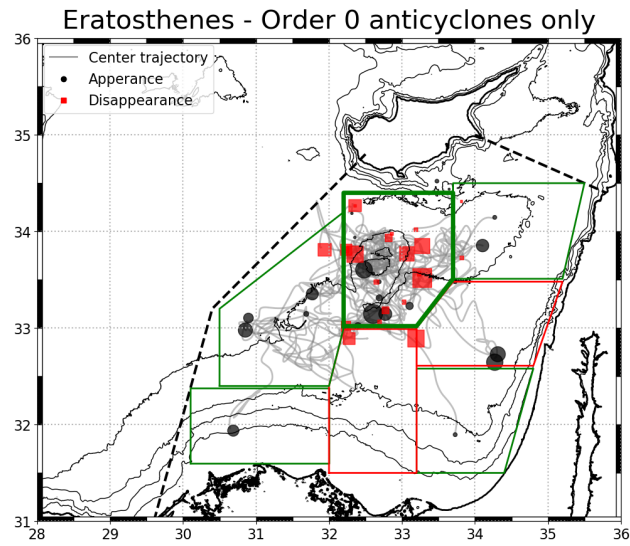
Figure A2. Appearance and disappearance locations for all *order 0* anticyclones, for the Eratosthenes region. Even if not all of them die within the region, they disappear very close to it.
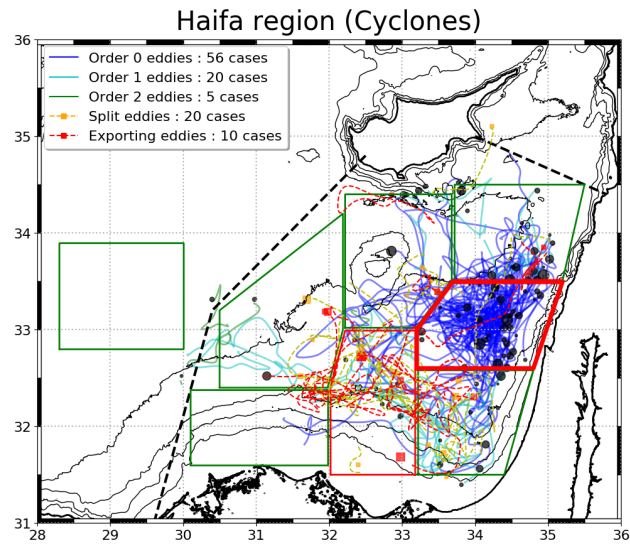
Figure A3. Cyclone transfers for Haifa region. Same as Fig. 6c but with Lagrangian convergence framework applied to cyclones. Boxes and dashed line are the same as in Fig. 3.

Table A1. Regions studied in the LB, with coordinates and area. Corresponding boxes are shown in Fig. 3.

Region	Eratosthenes	Beyrut	Haifa	Tel-Aviv	Port-Saïd	Herodotus	Nile	Mersa-Matruh
Box coordinates	33.0, 32.2	33.5, 33.7	32.6, 33.2	31.5, 33.2	31.5, 32.0	32.4, 30.5	31.6, 30.1	32.8, 28.3
	33.0, 33.2	34.5, 33.7	32.6, 34.8	32.6, 33.2	32.4, 32.0	33.2, 30.5	32.4, 30.1	32.8, 30.0
	33.5, 33.7	34.5, 35.5	33.5, 35.2	32.6, 34.8	33.0, 32.2	34.2, 32.2	32.4, 32.0	33.9, 30.0
	34.4, 33.7	33.5, 35.2	33.5, 33.7	31.5, 34.4	33.0, 33.2	33.0, 32.2	31.6, 32.0	33.9, 28.3
(° N , ° E)	34.4, 32.2		33.0, 33.2		31.5, 33.2	32.4, 32.0		
Area ($\times 10^3\, km^2$)	20.7	17.3	15.7	16.1	18.3	22.6	16.0	19.7

Table A2. Detail of *importing* and *exporting* anticyclones for the 7 regions of the Southeast LB identified in Sect. 3.2. Details are also shown in Fig. 6a-g, and the *net anticyclone gain* appears in Fig. 7.

Mean dynamical activity	Regions	Anticyclones born	Importing				Net Anticyclone gain	Exporting	
			Order 0	Order 1	Order 2	Total		Split	Merging
AC region	Eratosthenes	14	23	19	2	44	30	7	0
	Beyrut	29	38	1	0	39	10	2	2
	Tel-Aviv	29	29	0	0	29	0	0	3
	Nile	53	52	2	0	54	1	6	1
	Herodotus	42	54	2	0	56	14	2	8
CY region	Haifa	24	18	1	0	19	-5	0	6
	Port-Said	11	23	7	1	31	20	1	4